Journal of Thermal Analysis and Calorimetry (2023) 148:10505–10513
https://doi.org/10.1007/s10973-023-12330-x

# Calorimetric analysis of Mg–Li ultra light magnesium alloy

**Mariusz Król**[1] · **Jiří Hajnyš**[2]

Received: 20 December 2022 / Accepted: 15 June 2023 / Published online: 5 July 2023


**Abstract**
The Thermal-Derivative Analysis, or Computer-Aided Cooling Curve Analysis, is a commonly used method for determining the solidification parameters of metals and alloys. Knowledge of the enthalpy, kinetics and broad characteristics of the transformations taking place during the cooling of an alloy can be obtained with the proper configuration of analytical equipment and arrangement of test techniques. This work practically analyses the changes occurring in the Mg–4.5Li–1.5Al alloy as a result of the modification of the structure by the addition of TiB and Sr. The results indicate that adding grain refinements significantly affects the microstructure and thermal parameters of Mg–4.5Li–1.5Al alloy. The nucleation temperature and solidus temperature decrease with the addition of chemical reagents. Compressive strength improved due to the refinement of grain size. The results confirmed that thermal-derivative analysis is suitable for analysing changes in cast magnesium alloys.

**Keywords** TDA · CA-CCA · Magnesium–lithium alloy · Phase transformation kinetics · Grain refinement

## Introduction

The last 15 years have seen intensive development of Mg alloys, which has resulted in the development of new alloys and manufacturing technologies. Many new magnesium casting alloys with improved castability and enhanced performance properties have been developed. The development of magnesium alloys with desirable properties such as high mechanical strength, ductility, or creep resistance has been dynamized and directed mainly by the automotive industry [1].

Interest in lightweight engineering materials such as magnesium alloys is growing steadily. Recipients of magnesium alloys include the aerospace, medical, sports, and electronics industries (mobile phone and laptop computer housings), but the automotive industry is emerging as the main customer, with a steady increase in the number of components manufactured from Mg alloys, reducing the mass of vehicles, which has a significant impact on reducing fuel consumption and emissions of harmful exhaust fumes into the atmosphere. To date, the most considerable number of Mg alloy components have been used in the powertrain and interior of passenger vehicles, which have been obtained through various casting processes: casting mould, gravity casting, high-pressure casting, thixo-casting, and re-casting. In contrast, the greatest challenge for research centres and automotive concerns is using magnesium alloys for chassis and body components that would meet the safety requirements for passenger vehicles. To this end, research is being conducted into developing new casting and remolding alloys, improving advanced casting technologies, and, above all, using plastic processing (rolling, forging, extrusion), which allows better performance properties to be obtained. Another critical issue is the need to develop technologies for joining Mg alloy components and other materials and to develop coatings that provide adequate corrosion protection and wear resistance [2-5].

Magnesium and its alloys are characterized by a tendency to form a coarse-grained microstructure in castings combined with high grain heterogeneity. A coarse-grained alloy microstructure is disadvantageous because of the difficulties associated with possible plastic processing and the lower mechanical properties of the finished products. Pressure casting offers the possibility of obtaining a fine-grained microstructure due to the high undercooling of the alloy

✉ Mariusz Król
mariusz.krol@polsl.pl

[1] Department of Engineering Materials and Biomaterials, Faculty of Mechanical Engineering, Silesian University of Technology, Konarskiego 18a St., 44-100 Gliwice, Poland

[2] Center of 3D Printing Protolab, Department of Machining, Assembly and Engineering Technology, Faculty of Mechanical Engineering, VSB-TU Ostrava, 17. Listopadu 2172/15, 708-00 Ostrava-Poruba, Czech Republic

during solidification. However, the crystallization speed is much lower, especially for sand castings, die castings, and ingots intended for plastic processing. Therefore, a modification process involving the introduction of modifiers into the liquid alloy to obtain a fine-grained microstructure of the castings plays an essential role in magnesium alloy technology [1-7].

One way of obtaining a coarse-grained microstructure is to anneal at a temperature above the melting point, which was patented in 1931. The liquid metal is heated to 180–300 °C above the liquids temperature, annealed at this temperature for a short period (approx. 30 min), and then rapidly cooled to the correct casting temperature, followed by casting. During cooling, a large number of crystallization nuclei are formed, and a fine-grained microstructure is a result. This process is determined primarily by the chemical composition of the alloy and the technological parameters of the process. The fineness of the grains is more significant in alloys with Al content > 8% compared to alloys with low aluminium content. The best grain refinement effect is obtained when the liquid alloy is heated and annealed at 850–900 °C. The long annealing time of the alloy at this temperature does not affect the microstructure of the casting. In contrast, remelting causes a loss of the grain fragmentation effect in the casting [8, 9].

Another method currently being investigated is grain fragmentation by introducing the following elements into liquid magnesium alloys: Sr, Si, Ca, B, rare earth metals, and the compounds AlN, MgO, $TiB_2$, and TiC to form crystallization nuclei. Strontium is a typical modifier of mg alloys, where effective modification occurs after adding about 0.008–0.04 mass%. Strontium causes less modification effects than sodium, but it is less sensitive to the so-called over modification phenomenon, which leads to a deterioration of the mechanical properties. A higher strontium concentration causes surface defects in the form of pores, especially in areas of thicker cross-section, where crystallization is slower. Increased strontium content can also hinder the outgassing process of the alloy and favor the formation of fine precipitates that cause a deterioration of the tensile strength and lower ductility of magnesium alloys [10-13].

Titanium is most often used in combination with boron to alter the morphology of certain primary separations. An excess of titanium in the stoichiometric compound $TiB_2$ is necessary to achieve a suitable crystal fragmentation effect. Titanium is used in higher concentrations for a fine-grained structure to reduce the tendency for hot cracking of magnesium castings [14].

One way to evaluate the structure modification is to use thermal-derivative analysis, which visualizes the transformations occurring during the alloy crystallization process. The crystallization of metal alloys is best represented by thermal analysis and preferably by the ATD method. The theory behind the technique is that a signal form cooling curve is recorded, and the first derivative of the temperature is determined. Crystallization begins when the first derivative does not coincide with the base curve, which represents the absence of crystallization and heat release during the solidification of the alloy. The most incredible intensity of heat release is lost at the maximum of the derivative. When it assumes a minimum value (sometimes less than zero), the beginning of crystallization of the next phase or the end of alloy crystallization occurs [13-17].

The presented work focuses on calorimetric analysis of Mg–Li alloys with chemical agents (Titanium/Boron and Strontium) that facilities nucleation of new magnesium crystals.

## Experimental procedure

The ultralight magnesium-lithium alloy was selected from the group of Mg–Li foundry alloys based on the Mg–Li binary phase diagram (Fig. 1), characterized by a single α-Mg phase structure. The chemical composition of the Mg–4.5Li–1.5Al cast alloy analyzed in the work, which was examined using an ICP-OES Optima 5300 V inductively coupled plasma optical emission spectrometer from PerkinElmer, has been presented in Table 1. Ingots of high-purity magnesium (min. 99.5%), lithium (99.9%), aluminum (99.98%) and TiB and AlSr reference alloys, used as grain modifiers, were melted in the temperature interval of 700–720 °C at a pressure of 650 torr in a mild steel crucible using a VSG 02 induction heater supplied by Balzers. A protective atmosphere of argon was used during the melting process. In the final stage of alloy preparation, the liquid metal was cast by gravity into a graphite mould.

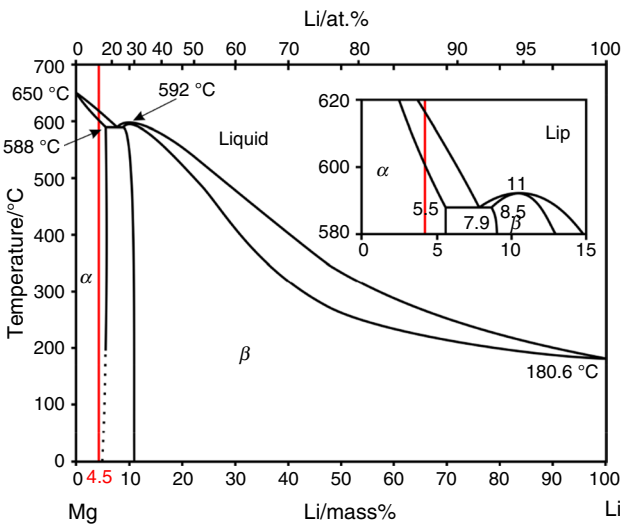


**Fig. 1** Mg–Li binary phase diagram

**Table 1** Chemical composition of analysed materials (mass%)

| Element | Li | Al | Si | B | Ti | Sr | Mg |
|---|---|---|---|---|---|---|---|
| Mg–4.5Li–1.5Al | 4.64 | 1.86 | – | – | – | – | Rest |
| Mg–4.5Li–1.5Al + 0.2TiB | 4.66 | 1.80 | 0.0052 | 0.0019 | 0.0069 | – | Rest |
| Mg–4.5Li–1.5Al + 0.2Sr | 4.63 | 1.80 | 0.030 | – | – | 0.019 | Rest |
| Mg–4.5Li–1.5Al + 0.2TiB + 0.2Sr | 4.63 | 1.85 | 0.041 | 0.0012 | 0.0042 | 0.021 | Rest |
| TiB master alloy | – | Rest | 0.06 | 0.95 | 4.9 | – | – |
| AlSr10 master alloy | – | Rest | 0.08 | – | – | 10.7 | – |

The CNC machined samples in cylindrical shape in diameter of 18 mm and height 20 mm were subjected for the thermal-derivative analysis to register a crystallization process. The TDA analysis was performed on Universal Metallurgical Simulator and Analyser (UMSA) as follows: heating to 700 °C with heating rate 5 °Cs$^{-1}$, holding for 180 s and cooling to ambient temperature with cooling rate approx. 0.6 °Cs$^{-1}$. During the crystallization process, the calibrated K-type thermocouples (chromel–alumel) linked to a personal computer featuring high-speed NI data acquisition system has been used. The signal from thermocouple located at centre of analysed sample during heating and cooling cycles were registered with frequency of 5 Hz. The Fityk software was applicated to convert registered signal to first and second derivative curve to calculate latent heat and analyse crystallization process of alloys. At least four thermal analysis cycles were made for each alloy. To estimate fraction solid during crystallization process, the base line was calculated and plotted by 6th order function $(dT/dt)_{BL} = P_0 + P_1T + P_2T^2 + P_3T^3 + P_4T^4 + P_5T^5 + P_6T^6$ using the Newtonian method for selected data points comes from 1st derivative of cooling curve before the nucleation temperature and after the end of crystallization process of metal casts.

After the thermal-derivative analysis, the cylindrical samples with 10 mm height and 5 mm diameter were CNC machined for compression tests according to the DIN 50106 standard. Compressive tests were has been done on universal testing machine Z100 model from Zwick/Roell. The constant rate of cross-head displacement, during the tests was deployed. The load cell with 100 kN capacity was carried out during the compression tests. The compression test was aborted when a notable decrease in load was achieved, indicating that the samples is fractured.

The XRD analysis was carried out on an X'Pert diffractometer using a Co target, with a scan rate of 0.03 steps$^{-1}$ and a scan range of 2 h of 30°–110° was used.

For microstructure observation, the samples were ground on SiC paper and, in the next step, polished with diamond slurry and colloidal silica (OP-U-40 µm) and finally etched with an aqueous oxalic acid solution. Microstructures and grain size were analyzed using a Zeiss Axio Observer Z1 optical microscope and ImageJ image processing software.

## Results and discussion

High-tech manufacturing processes involves high production rates and in order to take advantage of the more advanced processes, high quality and selected properties of the ingot or strip material.

In magnesium alloys many of the desired properties developed during the short period of solidification and are maintained or even enhanced during the subsequent cooling period or heat treatment. Thus it is increasingly important to understand the domination mechanism which come into action during solidification and how they affect the crystal structure and morphology in the as cast metal. Such knowledge makes it possible to control some of the parameters which influence the solidification process on a beneficial way.

X-ray spectra of Mg–4.5Li–1.5Al alloys with different degrees of refinement are shown in Fig. 2. XRD peaks can be indexed as $\alpha$-Mg. By changing the grain size fineness, the phase composition does not change. The results are in agreement with the previous findings [14].

The cooling curves recorded for Mg–4.5Li–1.5Al alloys with different addition of grain modifiers in more detail are presented in Fig. 3. Regarding changes in the slope of

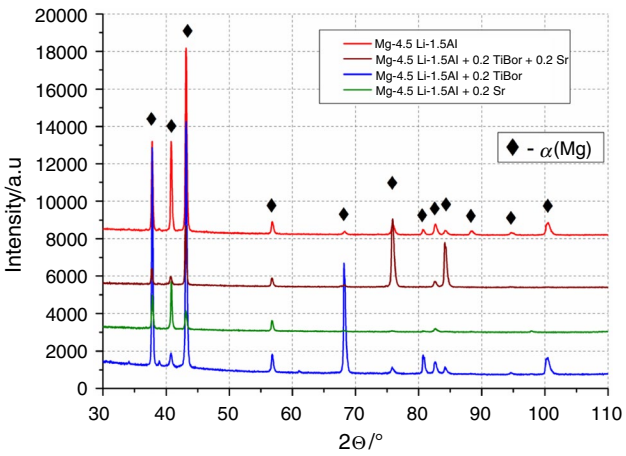


**Fig. 2** X-ray diffraction patterns of investigated alloys

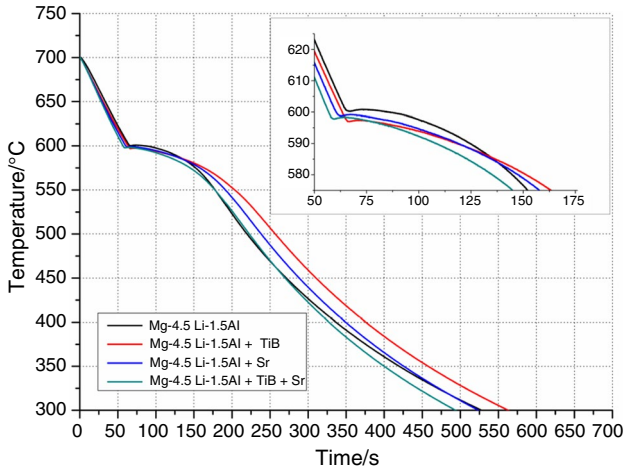


**Fig. 3** Effect of different grain modifiers on cooling curves of analysed alloys

the cooling curves, one visible stage defines the different phase formation temperatures in the alloy system. The phase response is related to forming a dendritic primary α-Mg network. As seen in Table 2, the appearance temperatures of the various phases are shifted when the different grain modifiers have been added. The metal starts solidifying slowly at the equilibrium temperature since no sufficient nuclei are present. A certain undercooling is necessary to provide the driving force for nucleating and growth processes. In the first stage, the liquid metal must be undercooled to the real nucleation temperature ($T_N$), where nucleating particles, inherently occurring in the liquid metal, evolve actively. When those particles grow into small crystals, the latent heat is generated, increasing the surrounding melt temperature.

The magnesium-lithium alloys, being an Mg–Li hypoeutectic alloy, have the following typical precipitation sequence: formation of a dendritic network of *a*-magnesium and followed by the precipitation of other more complex phases like $\eta$(LiAl) in alloys with aluminium [14]. In Fig. 4, characteristics cooling curves are presented, and their first derivatives for the samples from a primary alloy and the samples from the modified alloy by adding TiB and Sr for the solidification case moulds. Moreover, the region among the zero line or as called the base line, and the first derivative, calculated by the Newtonian method, corresponds to the volume of latent heat emitted when solid phase nuclei are formed from liquid metal. The first magnesium dendrites formation, corresponding to the first peak presented in all cooling curves, occurred approximately at 606 °C in the Mg–4.5Li–1.5Al primary alloy. In contrast, after the addition of grain refinements, this peak decreases to around 602 °C, independently of the type of grain modifiers.

Analyzing Fig. 4 and the results presented in Table 2, when 0.2% TiB is added, the $T_N$ temperature increases slightly from 606 to 608 °C. When 0.2% Sr and 0.2TiB and 0.2TiB + 0.2Sr are added to the alloy, the $T_N$ temperature of Mg–4.5Li–1.5Al decreases to 605 and 602 °C, respectively. The primary reason for this phenomenon is associated with the heat release rate. From this point of view, adding grain modifiers releases more heat, and the liquid alloy is cooled to a temperature lower than the equilibrium melting point. This condition ensures the appearance of more potential substrates for nucleation due to the existing suitable crystallization nuclei. Thus, nucleation continues easily and quickly [17]. The second theory is that diffusion kinetics reduces the nucleation temperature. The third theory states that due to the appearance of elements with reduced thermal conductivity, the $T_N$ of the analyzed alloys decreases due to a reduction in the total thermal conductivity of the alloy and an increased temperature gradient in the liquid metal [18].

Undercooling of the alloy ($\Delta T$) as a result of the difference between nucleation temperature ($T_N$) and minimum temperature ($T_{Min}$), being one of the two crucial parameters providing microstructural changes, especially grain modification of $\alpha$-Mg, indicates the limitation for growing the $\alpha$-Mg phase. The $\Delta T$ was calculated at 5.78, 10.87, 6.5 and 4.69 °C for Mg–4.5Li–1.5Al, Mg–4.5Li–1.5Al + 0.2TiB, Mg–4.5Li–1.5Al + 0.2Sr and Mg–4.5Li–1.5Al + 0.2TiB + 0.2Sr alloys, respectively.

The dendrite coherency point (DCP) is where dendritic networks become coherent. From the foundry industry point

**Table 2** Characteristic parameters for crystallization of the analyzed Mg–Li–Al alloys

| | Reaction/°C | Mg–4.5Li–1.5Al | Mg–4.5Li–1.5Al + 0.2TiB | Mg–4.5Li–1.5Al + 0.2Sr | Mg–4.5Li–1.5Al + 0.2TiB + 0.2Sr |
|---|---|---|---|---|---|
| 1 | $T_N$—nucleation temperature (liquidus temperature) | 606.06 | 607.9 | 605.3 | 602.5 |
| 2 | $T_{Min}$—minimum temperature | 600.28 | 597.0 | 598.8 | 597.8 |
| 3 | $\Delta T$—undercooling | 5.78 | 10.9 | 6.5 | 4.7 |
| 3 | $T_{DCP}$—Temperature at Dendrite Coherency Point | 600.7 | 597.4 | 599.2 | 598.3 |
| 4 | $T_{\alpha,G}$—growth temperature of $\alpha$-Mg | 600.5 | 597.3 | 599.1 | 598.1 |
| 5 | $T_{\eta(LiAl)}$-nucleation of $\eta$(LiAl) phase | 545.4 | 554.5 | 542.5 | 543.6 |
| 6 | $T_{SOL}$—temperature at end of solidification | 524.2 | 492.3 | 493.2 | 491.2 |

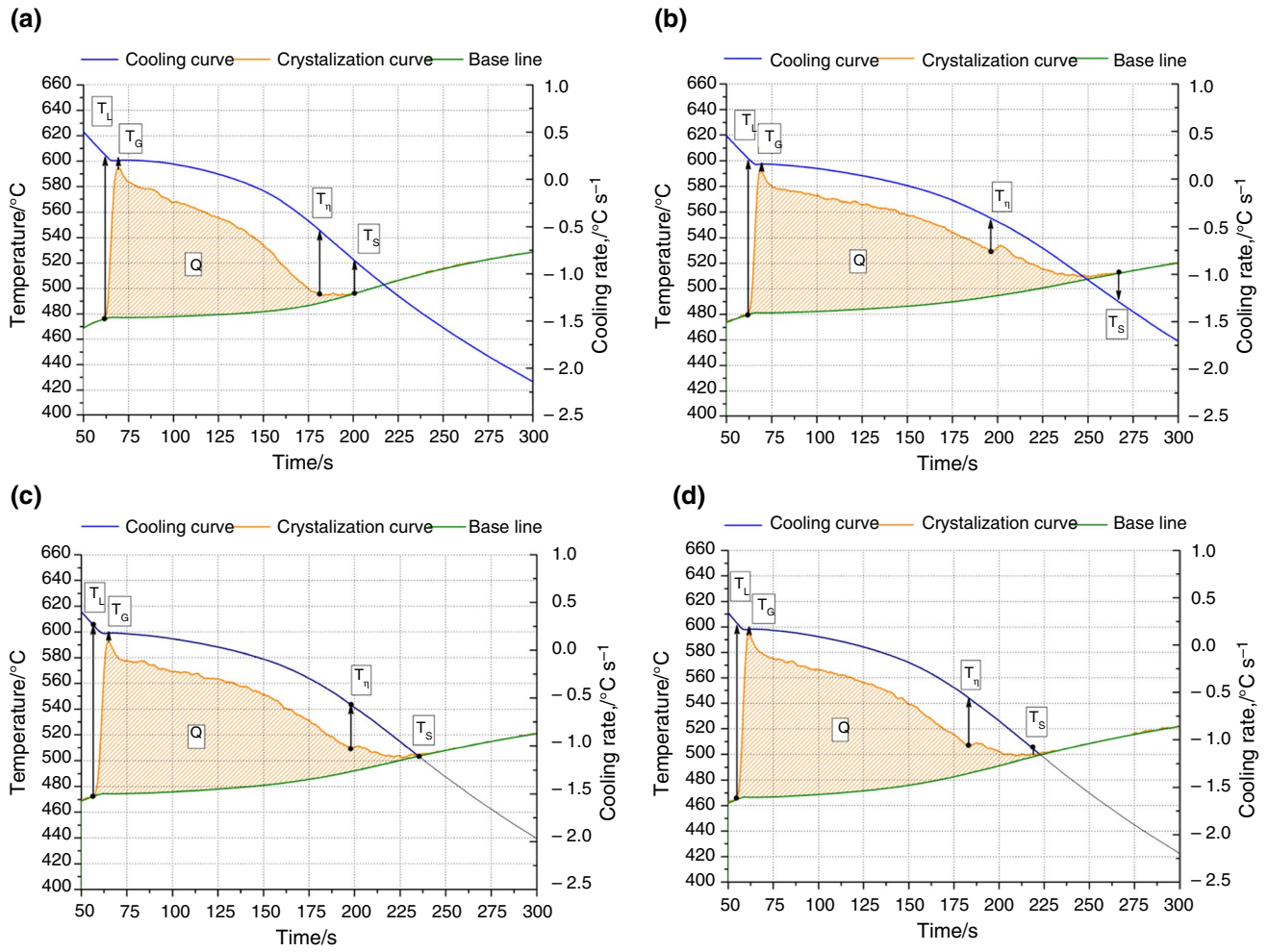


**Fig. 4** Results of TDA of: **a** Mg–4.5Li–1.5Al, **b** Mg–4.5Li–1.5Al + 0.2TiB, **c** Mg–4.5Li–1.5Al + 0.2Sr, **d** Mg–4.5Li–1.5Al + 0.2TiB + 0.2Sr

of view is very important because it indicates the possibility of developing casting defects such as macro segregation, shrinkage, porosity, and hot tearing in casting alloys. In utilized thermal analysis, one thermocouple measure has been used at centre of tested alloy, and appointing of minimum point on the second derivative curve determined DCP temperature characteristics. The one thermocouple measurement method, unlike other mechanical or thermal measurement methods, allows to save money and time for $T_{DCP}$ analysis. Figure 5 illustrates the cooling plots of the analyzed alloys recorded during thermal analysis and the calculated second derivative line to determine the dendrite cohesion point and associated temperature. The temperature of the DCP and the amount of solid fraction in the DCP is related to grain size. In the case of solidification of castings, free dendrite growth occurs when the dendrites are not in contact with each other, and the dendrite becomes thicker when dendrite cohesion is reached. As presented in Table 2, the $T_{DCP}$ of grain modified alloys occurred at 600.7, 597.4, 599.2 and 598.3 °C for Mg–4.5Li–1.5Al, Mg–4.5Li–1.5Al + 0.2TiB, Mg–4.5Li–1.5Al + 0.2Sr and Mg–4.5Li–1.5Al + 0.2TiB + 0.2Sr alloys, respectively. The temperature at the dendrite coherence point decreases slightly for all grain-modified alloys than unmodified ones.

The solid fraction of analysed alloys has been calculated as a total region between the base line and first derivative. Analysis of fraction solid at DCP of unrefined Mg–Li alloys reach 9%, while addition of grain refinements cause decrease of fraction solid at dendrite coherency point, i.e. 4.8, 7.5 and 8.5% for alloys Mg–4.5Li–1.5Al + 0.2TiB, Mg–4.5Li–1.5Al + 0.2Sr and Mg–4.5Li–1.5Al + 0.2TiB + 0.2Sr respectively. The highest reinforcement effect has been achieved for alloy modified by TiB.

After formation of dendritic network of magnesium, around 545 °C is followed by precipitation of η(LiAl) from the residual liquid until the end of solidification. When 0.2 mass% of TiB has been added to the Mg–4.5Li–1.5Al

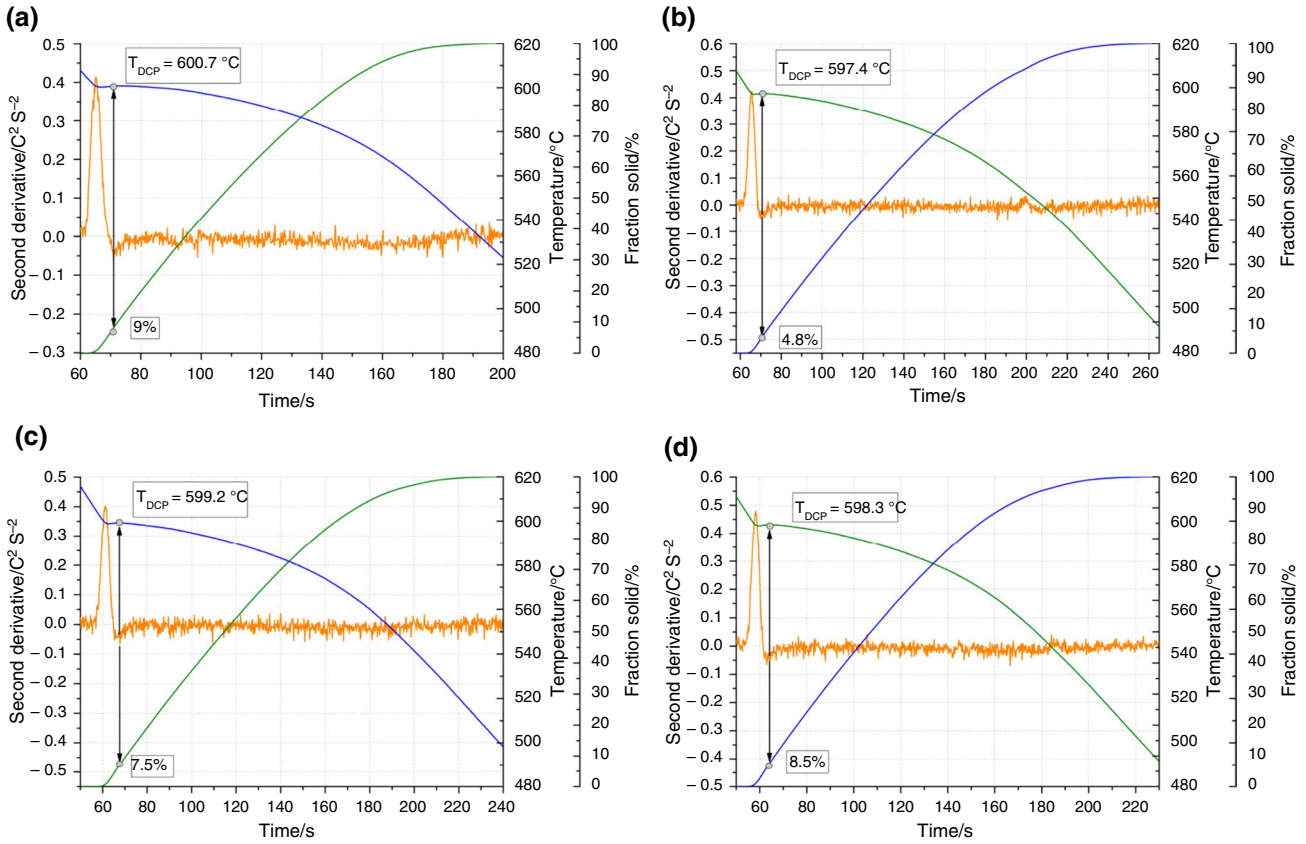


**Fig. 5** Cooling, second derivative and corresponding solid fraction curves for: **a** Mg–4.5Li–1.5Al, **b** Mg–4.5Li–1.5Al + 0.2TiB, **c** Mg–4.5Li–1.5Al + 0.2Sr and **d** Mg–4.5Li–1.5Al + 0.2TiB + 0.2Sr

alloy, the precipitation of η(LiAl) started at a higher temperature (554 °C). Titanium/Boron and Strontium addition negligible influenced on the precipitation of η(LiAl).

The last phase of crystallization process of the Mg–Li alloys presents a typical peak characterizing the end of solidification at 524 °C, while grain-modified alloys showed a tendency to decrease the solidification temperature to approximately 491 °C for alloy with 0.2TiB + 0.2Sr, cause the range of solidification temperature increases. It must be noted that the solidification temperature range is essential parameter for rheo- and thixocating.

The heat transport equation including latent heat evaluation was calculated:

$$\rho C_{\mathrm{p}} \frac{\mathrm{d}T}{\mathrm{d}t} = \nabla(\kappa \nabla T) + \rho \Delta H \frac{\mathrm{d}f_{\mathrm{s}}}{\mathrm{d}t} \tag{1}$$

where $\rho$ is the density, $C_{\mathrm{p}}$—the specific heat, $T$—the temperature, $t$—the time, $\kappa$ —the heat conductivity, $\Delta H$—the latent heat and $f_{\mathrm{s}}$ is the fraction solid. The expression can be divided in two parts, where the first part of which is independent of latent heat evaluation. When no solidification occurs, i.e. before and after solidification, the $\Delta H$ is zero, and under these conditions the heat flow out from the sample is proportional to d$T$/d$t$. Therefore, this derivative can be used as a measure of the rate of heat transfer from the sample. Using a least square approximation on the derivative

**Table 3** Thermal characteristics of analysed alloys

| | Liquid heat capacity $Cp_l$/ $Jg^{-1}$ °$C^{-1}$ | | Solid heat capacity $Cp_s$/$Jg^{-1}$ °$C^{-1}$ | |
|---|---|---|---|---|
| | 1.364 | | 1.137 | |
| Analysed alloy | Mg–4.5Li–1.5Al | Mg–4.5Li–1.5Al + 0.2TiB | Mg–4.5Li–1.5Al + 0.2Sr | Mg–4.5Li–1.5Al + 0.2TiB + 0.2Sr |
| Latent heat of sample $Q$/J | 1075 | 1467 | 1495.5 | 1376.0 |
| Latent heat per gram/$Jg^{-1}$ | 139 | 185 | 179 | 178 |

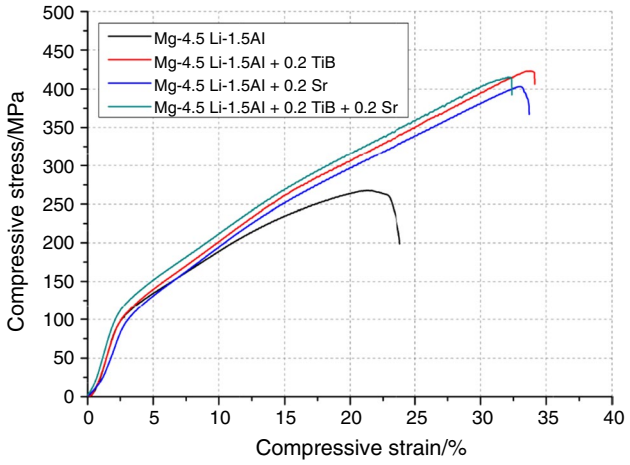


**Fig. 6** Stress versus strain curves of the analysed materials

as a function of temperature before and after solidification, the heat flow out form the system can be calculated at each moment during solidification, provided the actual temperature/time relation has been properly recorded [17].

The quantity of latent heat emitted during crystallization of liquid metal is presented in Table 3. The latent heat of the crystallization of the Mg–4.5Li–1.5Al during cooling sequence was 139 $Jg^{-1}$. Crystallization of the alloy with the grain refiner as TiB caused increase in latent heat to 185 $Jg^{-1}$ where addition of Sr and TiB + Sr caused increase in latent heat to approx. 178 $Jg^{-1}$. The latent heat can be corelated to the grain size of analysed alloys. When alloys are refined more, more latent heat is emitted during crystallisation due to the greater number of crystallisation nuclei.

The line intersect method characterised the grain size of analysed samples to evaluate the effects of grain reagents on the Mg–4.5Li–1.5Al cast alloy. Modification of the Mg–4.5Li–1.5Al alloy with 0.2 mass% TiB causes a decrease in grain size from 996 ± 200 to 523 ± 100 µm—the addition of 0.2 mass% Sr reduces the grain size of the alloy to 630 ± 70 µm, while the simultaneous addition of TiB and Sr causes a decrease in grain size of approx—439 ± 80 µm.

The stress vs strain plots of the as-cast alloys are shown in Fig. 6. The unmodified Mg–Li alloy is characterised by yield stress of ~ 100 MPa and expressive strain-hardening. A peak stress of approx. 267 MPa was recorded at a strain of ~ 21%, and a decrease in stress was noted in the next stage. This evident softening is assigned to the appearance of a fracture in the tested sample. The Mg–Li alloys modified by 0.2% TiB exhibit lower yield stress approx. 95 MPa than the unmodified alloy, but a with comparable strain hardening. Peak stress was followed at ~ 422 MPa at a strain of ~ 33%, followed by an evident sudden decrease in stress generated by the fracture of the tested sample. The applied grain modifiers influence the compressive strength of analysed alloys. The compressive strength of analysed alloys modified with Sr and TiB and Sr simultaneously was 404 MPa and 414 MPa, respectively.

Figure 7 shows a view of the surface topography after the compression test. The fracture surfaces are characterised by

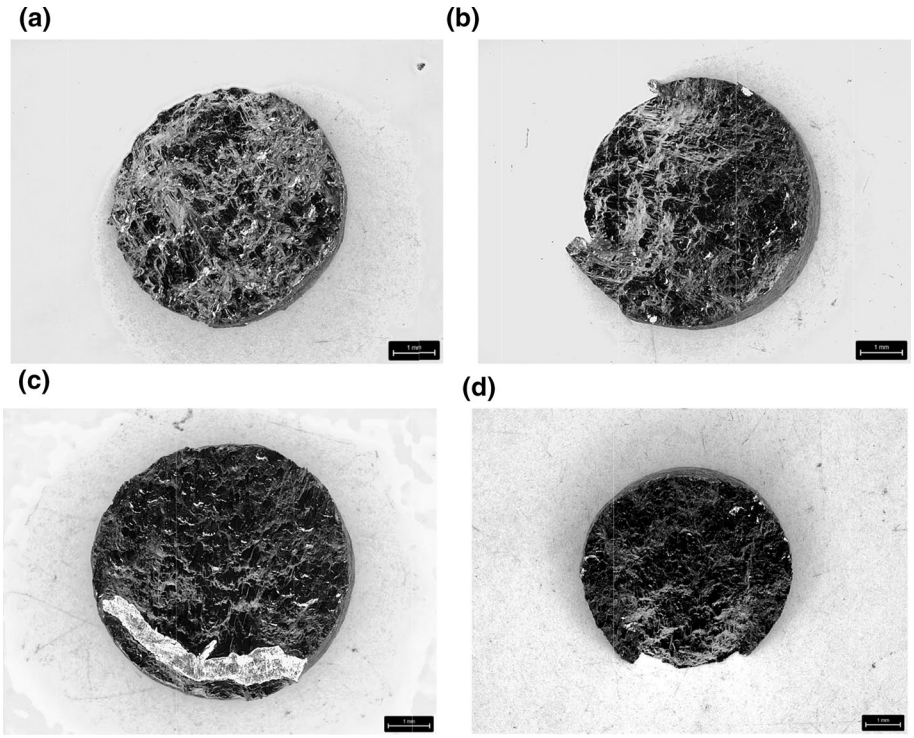


**Fig. 7** Fracture surface of material: **a** Mg–4.5Li–1.5Al, **b** Mg–4.5Li–1.5Al + 0.2TiB, **c** Mg–4.5Li–1.5Al + 0.2Sr, **d** Mg–4.5Li–1.5Al + 0.2TiB + 0.2Sr

a mixed morphology with both cleavage and particle necks ductile fracture (Fig. 6a), which is more evident in alloy after modification of TiB (Fig. 6b). The fracture track is varied. In the same area, very different behaviours can exist (Fig. 6c) and inter and intra particle (Fig. 6d). In addition, characteristic features of fragile fractures, such as cliffs and quasi-cleavage, are located within the ductile area, indicating a distinctive aspect (Fig. 6a). It was also noted that all the examples analysed show rupture in regions of apparent shear concentration. This means considerable deformation was generated in the area before the crack [19-21].

## Conclusions

The influence of grain modifiers on crystallization, grain size and mechanical properties of Mg–4.5Li–1.5Al alloy is presented. The obtained results can be summarized as follows:

1. Crystallization process are influenced by the applied grain modifiers. Addition of the TiB and Sr, causes in the reduction of the nucleation temperature and solidus temperature from 606 to 602 and 524 to 491 °C, respectively.
2. The latent heat of analysed alloy emitted during crystallization process of Mg–Li–Al increases with addition of grain modifiers. When the TiB is added, the latent heat increases from 139 to 185 $Jg^{-1}$, with addition Sr and TiB and Sr simultaneously, the latent heat increases to 179 and 178 $Jg^{-1}$, respectively.
3. The fraction solid at coherency point decrease after modification by TiB and AlSr grain refinements.
4. Refining ultralight Mg–Li alloys with TiB and Sr allows for an appropriate variety of strengths that can be adopted for numerous applications.
5. Topography of fracture surfaces in analysed grain-refined Mg–Li alloys treated with different chemical reagents, revealed two main fracture mechanisms: ductile and brittle fracture.

**Acknowledgements** Work has been done in connection with project Innovative and additive manufacturing technology—new technological solutions for 3D printing of metals and composite materials, Reg. No. CZ.02.1.01/0.0/0.0/17_049/0008407 financed by Structural Founds of Europe Union.

**Author contributions** All authors contributed to the study conception and design. Material preparation, data collection and analysis were performed by MK, and JH. The first draft of the manuscript was written by MK and all authors commented on previous versions of the manuscript. All authors read and approved the final manuscript.



## References

1. Divya PVS, Penumakala PK, Nallathambi AK. Infuence of secondary cooling strategies on thermal gradients in the direct chill casting of magnesium alloys. J Therm Anal Calorim. 2022;147:203–18. https://doi.org/10.1007/s10973-020-10235-7.
2. Luo X, Dang S, Kang L. Compression deformation behavior of AZ81 magnesium alloy at elevated temperatures. Adv Mater Sci Eng. 2014. https://doi.org/10.1155/2014/717452.
3. Yavari F, Shabestari SG. Effect of cooling rate and Al content on solidification characteristics of AZ magnesium alloys using cooling curve thermal analysis. J Therm Anal Calorim. 2017;129:655–62.
4. Krol M, Tanski T, Sitek W. Thermal analysis and microstructural characterization of Mg-Al-Zn system. In Alloys 3rd international conference on modern technologies in industrial engineering (ModTech) 2015 Modern technologies in industrial engineering (Modtech2015) 95. https://doi.org/10.1088/1757-899X/95/1/012006
5. Tański T, Pakieła W, Janicki D, Tomiczek B, Król M. Properties of the aluminium alloy EN AC-51100 after laser surface treatment. Arch Metall Mater. 2016;1:199–204.
6. Sroka M, Nabiałek M, Szota M, Zieliński A. The influence of the temperature and ageing time on the $NiCr_{23}Co_{12}Mo$ alloy microstructure. Rev Chim-Bucharest. 2017;4:737–41. https://doi.org/10.37358/RC.17.4.5541.
7. Zieliński A, Sroka M, Dudziak T. Microstructure and mechanical properties of Inconel 740H after long-term service. Materials. 2018;11:2130. https://doi.org/10.3390/ma11112130.
8. Guo E, Wang L, Feng Y, Wang L, Chen Y. Effect of cooling rate on the microstructure and solidification parameters of Mg–3Al–3Nd alloy. J Therm Anal Calorim. 2019;135:2001–8.
9. Bassani P, Gariboldi E, Tuissi A. Calorimetric analysis of AM60 magnesium alloy. J Therm Anal Calorim. 2005;80:739–47.
10. Barrena MI, Gomez de Salazar JM, Pascual L, Soria A. Determination of the kinetic parameters in magnesium alloy using TEM and DSC techniques. J Therm Anal Calorim. 2013;113:713–20. https://doi.org/10.1007/s10973-012-2791-7.
11. Snopiński P, Matus K, Tatiček F, Rusz S. Overcoming the strength-ductility trade-off in additively manufactured AlSi10Mg alloy by ECAP processing. J Alloys Compd. 2022. https://doi.org/10.1016/J.JALLCOM.2022.165817.
12. Snopiński P, Król M, Pagáč M, Petrů J, Hajnyš J, Mikuszewski T, Tański T. Effects of equal channel angular pressing and heat treatments on the microstructures and mechanical properties of selective laser melted and cast AlSi10Mg alloys. Arch Civ Mech Eng. 2021;21:92. https://doi.org/10.1007/s43452-021-00246-y.
13. Dedavid BA, Costa EM, Ferreira CRF. A study of precipitates formation in aa 380.0 aluminium alloys modified by the addition of magnesium. J Therm Anal Calorim. 2002;67:473–80.

14. Król M. Magnesium–lithium alloys with TiB and Sr additions. J Therm Anal Calorim. 2019;138:4237–45. https://doi.org/10.1007/s10973-019-08341-2.
15. Poggiali FSJ, Figueiredo RB, Aguilar MTP, Cetlin PR. Effect of grain size on compression behavior of magnesium processed by equal channel angular pressing. J Mater Res Technol. 2013;2/1:30–5.
16. Shabestari SG, Malekan M. Thermal analysis study of the effect of the cooling rate on the microstructure and solidification parameters of 319 aluminum alloy. Can Metall Q. 2005;44:305–12.
17. Bäckerud L, Król E, Tamminen J. solidification characteristics of aluminium alloys. Vol. 1: Wrought Alloys, SkanAluminium, Oslo, Norway, 1986.
18. Farahany S, Ghandvar H, Nordin NA. Solidification characteristics of ex situ particulate-reinforced aluminum matrix composites. Int J Metalcast. 2023. https://doi.org/10.1007/s40962-023-01005-w.
19. Steglich D, Tian X, Bohlen J, Kuwabara T. Mechanical testing of thin sheet magnesium alloys in biaxial tension and uniaxial compression. Exp Mech. 2014;54:1247–2125.
20. Bidulský R, Bidulská J, Grande MA. Correlation between microstructure/fracture surfaces and material properties. Acta Phys Pol A. 2012;122(3):548–52.
21. Bidulský R, Bidulská J, Grande MA. Response of the Cr-alloyed PM steels on vacuum sintering and heat treatment. High Temp Mater Proc. 2013;32(5):467–73. https://doi.org/10.1515/htmp-2012-0174/html.